



This open access document is posted as a preprint in the Beilstein Archives at <https://doi.org/10.3762/bxiv.2024.59.v1> and is considered to be an early communication for feedback before peer review. Before citing this document, please check if a final, peer-reviewed version has been published.

This document is not formatted, has not undergone copyediting or typesetting, and may contain errors, unsubstantiated scientific claims or preliminary data.

**Preprint Title** Clays enhanced with niobium: potential in wastewater treatment and reuse as pigment with antibacterial activity

**Authors** Silvia Jaerger, Patricia Appelt, Mário A. A. da Cunha, Fabián C. Ayma, Ricardo Schneider, Carla Bittencourt and Fauze J. Anaissi

**Publication Date** 11 Sept. 2024

**Article Type** Full Research Paper

**Supporting Information File 1** BJ-ANANO-Supplementary-3nd vers.docx; 241.6 KB

**ORCID® IDs** Patricia Appelt - <https://orcid.org/0000-0003-4302-534X>; Carla Bittencourt - <https://orcid.org/0000-0002-3330-6693>; Fauze J. Anaissi - <https://orcid.org/0000-0002-5454-472X>



License and Terms: This document is copyright 2024 the Author(s); licensee Beilstein-Institut.

This is an open access work under the terms of the Creative Commons Attribution License (<https://creativecommons.org/licenses/by/4.0>). Please note that the reuse, redistribution and reproduction in particular requires that the author(s) and source are credited and that individual graphics may be subject to special legal provisions.

The license is subject to the Beilstein Archives terms and conditions: <https://www.beilstein-archives.org/xiv/terms>.

The definitive version of this work can be found at <https://doi.org/10.3762/bxiv.2024.59.v1>

# Clays enhanced with niobium: potential in wastewater treatment and reuse as pigment with antibacterial activity

Silvia Jaerger<sup>\*1,2</sup>, Patricia Appelt <sup>‡2</sup>, Mario Antônio Alves da Cunha <sup>‡3</sup>, Fabián Ccahuana Ayma <sup>‡2</sup>, Ricardo Schneider <sup>‡1</sup>, Carla Bittencourt <sup>‡4</sup>, Fauze Jacó Anaissi <sup>\*‡2</sup>

<sup>1</sup>Federal University of Technology - Paraná - UTFPR, Campus Toledo, Rua Cristo Rei, 19. 85902-490, Toledo, Brazil.

<sup>2</sup>Chemistry Department, Universidade Estadual do Centro-Oeste, Guarapuava 85040-167, PR, Brazil.

<sup>3</sup> Department of Chemistry, Universidade Tecnológica Federal do Paraná, Pato Branco 85503-390, Brazil;

<sup>4</sup> Chimie des Interactions Plasma-Surface (ChIPS), Research Institute for Materials Science and Engineering, University of Mons, 7000 Mons, Belgium

Email: Silvia Jaerger [sjaerger@gmail.com](mailto:sjaerger@gmail.com) and Fauze J. Anaissi [anaissi@unicentro.br](mailto:anaissi@unicentro.br)

\* Corresponding author

‡ Equal contributors

## Abstract

Raw smectite clay (SM) sourced from the Guarapuava region, Brazil, underwent modification with niobium oxide (SMOx) and niobium phosphate (SMPPh) to act as adsorbent and photocatalyst in the remediation of wastewater containing methylene blue (MB) dye. Additionally, these materials were evaluated for their potential as antibacterial hybrid pigments. The characterization of the SM, SMOx, and SMPPh samples was conducted using various analytical techniques to assess the modifications induced by the incorporation of niobium compounds into the clay matrix and to evaluate the colorimetric properties and dye removal efficiency. Notably, X-ray diffractometry (XRD), X-ray photoelectron spectroscopy (XPS), and laser-induced breakdown spectroscopy (LIBS) were used to detail characterization. The results indicate successful modification of SM through the intercalation of niobium oxide and niobium phosphate within the interlayer spaces of the clay structure. Following characterization, the SMOx and SMPPh samples were used for the treatment of solutions containing methylene blue at 25 °C. The initial concentration was 400 mg L<sup>-1</sup>. Subsequently, the efficacy of the dye removal was assessed using the minimum inhibitory concentration (MIC) assay against two bacteria strains: *Bacillus cereus* (ATCC 10876) and *Proteus mirabilis* (ATCC 35649). The analysis revealed remarkable antibacterial activity against *Proteus mirabilis*, suggesting a preferential selectivity for Gram-negative bacteria.

## Keywords

Smectite; niobium; adsorption; photocatalysis; hybrid pigment

## 1.0 Introduction

The most found dye pollutants in wastewater on a global scale originate from textile, plastic, paper, food, cosmetics, mineral, and pharmaceutical industries, among others, resulting in significant environmental impacts [1]. Dyes, as chemical compounds used to impart color to different materials, play a crucial role in industries requiring coloring, such as textile, food, cosmetics, rubber, printing, paper, and plastic. Globally, an estimated  $7 \times 10^5$  tons of dyes are produced, with 10-15% typically disposed of as wastewater waste [2]. Among the most used dyes, methylene blue (MB) is an intense blue cationic dye important in medical sciences, chemistry, and biology, as well as widely used in the textile industry [2]. Prolonged exposure to MB can result in adverse health effects, including abdominal disorders, respiratory distress, skin sensitization, and blindness [3]. The dark blue color of MB in wastewater reduces light penetration into aquatic organisms, disturbing the balance of the ecosystem and harming various forms of life [3]. Effluents and water bodies containing MB require prioritized treatment due to its adverse effect on water quality. Therefore, it is crucial to explore remedial strategies for MB, especially considering the water scarcity challenges that many countries face [3].

To satisfy environmental regulations, a range of wastewater treatment technologies with inherent advantages and limitations are available, encompassing processes such as advanced oxidation, extraction, and biodegradation [4]. Unfortunately, these methods exhibit inefficiencies due to the generation of secondary pollution and high operational costs. Biological and anaerobic degradation of dyes may yield carcinogenic by-products [4,5], highlighting the significant challenge in purifying water contaminated with dyes necessitating the development of cost-effective technologies for their removal from industrial effluents.

Adsorption emerges as a widely used method for pollutant removal from wastewater due to its design simplicity, operational ease, and relatively straightforward regeneration of adsorbent. Various adsorbents such as chitosan, cellulose, organophilic clays, kaolinite and montmorillonite clays, and activated carbon, among others, have been used for removing toxic compounds from polluted water [6]. Among these adsorbents, smectite clay exhibits advantageous properties as an adsorbent, characterized by its low cost, abundant availability, non-toxic nature, and large surface area [2,7]. Additionally, its negatively charged surface renders it favorable for the

adsorption of cationic [7]. In the region of Guarapuava, Paraná, Brazil, smectite clay is abundantly found. This natural clay has predominantly the smectite phase (at least 50%), known as montmorillonite. Isomorphic substitution of cations between the interlayer space of montmorillonites by exchanging  $\text{Na}^+$ ,  $\text{Ca}^{2+}$ ,  $\text{Mg}^{2+}$ , and  $\text{Cu}^{2+}$  cations add other functionalities to the resulting material [7].

Heterogeneous photocatalysis emerges as a cost-effective alternative to biological treatment methods for purifying polluted water [8]. Using semiconductors as heterogeneous catalysts proves to be more efficient compared to traditional methods, as the photocatalytic process gradually decomposes contaminating molecules without generating residues from the original organic matter, thus avoiding the disposal of sludge [8]. This approach allows the removal of various organic pollutants, including textile dyes, using solid semiconductors (for example,  $\text{NbOPO}_4$  and  $\text{Nb}_2\text{O}_5$ ) and photons (with energy greater than the band-gap energy of the semiconductor) to generate  $\text{OH}^\bullet$  radicals (strong oxidants), leading to the mineralization of organic pollutants, including textile dyes [8].

In this study, smectite clay samples modified with niobium oxide and niobium phosphate were characterized by X-ray diffractometry (DRX), vibrational spectroscopy (FTIR), spectroscopy in the ultraviolet-visible region (UV-Vis), X-ray photoelectron spectroscopy (XPS), static laser scattering (SLS), laser-induced breakdown spectroscopy (LIBS) and colorimetry (CIE  $L^*a^*b^*$ ). Subsequently, the as-prepared samples were evaluated for their color properties, and the niobium-modified samples were applied as adsorbents and MB dye photocatalysts. The novel-developed pigments, specifically the smectite clay modified with niobium-containing adsorbed dye, were investigated as antibacterial pigments. Additionally, colorimetric analysis of the synthesized pigments dispersed in paint was evaluated.

## 2.0 Experimental

### 2.1 Materials

The smectite clay from the Guarapuava region in the Parana State, Brazil, was purchased from a local supplier. Niobium phosphate ( $\text{NbOPO}_4$ ) and niobium pentoxide ( $\text{Nb}_2\text{O}_5$ ) were provided as donations by Companhia Brasileira de Metalurgia e Mineração (CBMM). Methylene blue, with molecular mass  $319.8513 \text{ g mol}^{-1}$ , was obtained from Nuclear (Brazil).

## 2.2 Clay modified with niobium

First, the clays were swollen; for this purpose, 2 g of smectite clay was dispersed in 100 mL of water, and the resulting suspension was kept under stirring for 24 h. Then, 3.14 g of niobium phosphate (NbOPO<sub>4</sub>) and niobium pentoxide (Nb<sub>2</sub>O<sub>5</sub>) were added. The clay/Nb suspension was continuously stirred for 72 hours at 65 °C. Finally, the suspensions, after being cooled to room temperature, were subjected to thermal treatment at 500 °C, with a heating rate of 5 °C/min. These samples were named SMPH and SMOx for modification with NbOPO<sub>4</sub> and Nb<sub>2</sub>O<sub>5</sub>, respectively.

## 2.3 Adsorption and photocatalysis tests

Before the adsorption and photocatalysis assessments, a stock solution of the MB dye was prepared at a concentration of 1 g L<sup>-1</sup>. The calibration analytical curve was established using a UV-Vis spectrophotometer at a wavelength of 664 nm.

Adsorption experiments were conducted in batches containing 250 mg of the SMPH and SMOx samples under agitation at 25°C. 100 mL of MB solutions at a concentration of 400 mg L<sup>-1</sup> were used for 3 hours. The adsorption experiment was carried out considering light ambient laboratory conditions. Following the adsorption process, the clay/Nb samples were centrifuged at 3500 rpm for 10 minutes, and the final concentration of the solutions was determined using a UV-vis spectrophotometer. These samples were named A-SMPH and A-SMOx for modification with NbOPO<sub>4</sub> and Nb<sub>2</sub>O<sub>5</sub>, respectively.

Photocatalytic tests were performed using 100 mL of an MB solution at a concentration of 400 mg L<sup>-1</sup>. In this experiment, 250 mg of the SMPH and SMOx samples were used as catalysts. The experimental setup system included a thermostatic Pyrex glass reactor at 25°C (open), a magnetic stirrer, and a UV lamp (253.7 nm, 15 W, 220 V) within a dark chamber. After 3 hours of exposure, the solutions were centrifuged at 3500 rpm for 10 minutes, and their final concentrations were determined using a UV-vis spectrophotometer. These samples were labeled as A-SMPH<sub>P</sub> and A-SMOx<sub>P</sub> for modification with NbOPO<sub>4</sub> and Nb<sub>2</sub>O<sub>5</sub>, respectively.

The adsorption efficiency of MB by the clays was calculated using Equation 1:

$$\%Remotion = 100 \cdot \frac{(c_0 - c_f)}{c_0} \quad \text{Equation 1}$$

where  $C_0$  ( $\text{mg L}^{-1}$ ) is the initial concentration of the solution,  $C_f$  ( $\text{mg L}^{-1}$ ) is the final concentration of the solution.

The efficiency of MB photodegradation ( $X\%$ ) was determined by Equation 2:

$$X(\%) = \frac{(M_0 - M_f)}{M_0} \cdot 100 \quad (\text{Equation 2})$$

where  $M_0$  and  $M_f$  are the concentrations of MB at the beginning and at the end of the photocatalytic test, respectively.

## 2.4 Dispersion of the pigments clay/Nb and clay/Nb/MB in colorless commercial paint

The samples A-SMPh, A-SMOx, A-SMPhP, and A-SMOxP were separated through centrifugation and dried in an oven at  $70^\circ\text{C}$ . The clay powders, clay/Nb, and clay/Nb/MB powders were tested as pigments in colorless commercial paint. For this purpose, a 10% (w/w) proportion of the pigments in colorless commercial paint was used. A sodium hydroxide solution ( $\text{NaOH}$ ,  $1 \text{ mol L}^{-1}$ ) was dripped onto the clay powders until reaching a pH between 8 and 10. Subsequently, this suspension was blended with the transparent paint. Plaster molds were painted with both colorless and pigmented paint. After the paint dried, the color was characterized through colorimetric analysis ( $\text{CIEL}^*a^*b^*$ ) and UV-Vis spectroscopy.

## 2.5 Antimicrobial activity test

The antimicrobial properties of the SMPh, SMOx, A-SMPh, A-SMOx, A-SMPhP, and A-SMOxP samples were investigated against the bacteria *Bacillus cereus* (ATCC 10876) (Gram-positive) and *Proteus mirabilis* (ATCC 35649) (Gram-negative). The samples of smectite clay modified with niobium were dispersed in water. The assay followed the protocols described by the Clinical and Laboratory Standards Institute (CLSI). The samples were evaluated using the minimum inhibitory concentration (MIC) method [26,27] at concentrations ranging from 1.25 to 0.09 mg/mL.

The bacterial stock cultures were activated by culturing in brain heart infusion (BHI) broth at  $37^\circ\text{C}$  for 24 hours. Then, the cellular concentrations were standardized according to the McFarland 0.5 scale ( $\cong 1.5 \times 10^8 \text{ CFU/mL}$ ) using a spectrophotometer at a wavelength of 625 nm in saline water tubes. Subsequently, 100  $\mu\text{L}$  of Mueller-

Hinton broth was added to all wells in 96-well plates, followed by duplicate addition of the samples using serial microdilution, and finally, 10  $\mu\text{L}$  of the inoculum. The plates were then incubated for 24 hours at 37°C. After incubation, 20  $\mu\text{L}$  of the TTC dye (0.125% w/v - 2,3,5-triphenyltetrazolium chloride 0.125%) (NEON®) was added to all wells, and the plate was kept in an oven for an additional two hours. The antibacterial activity was determined by MIC, observing the presence/absence of viable bacteria due to the reaction of the TTC dye with the enzyme succinate dehydrogenase (present in the mitochondria), leading to the formation of a salt called Formazan with a pink-reddish color.

## 2.6 Characterization

X-ray diffraction (XRD) measurements of the powder were conducted using a Rigaku SmartLab SE 3kW diffractometer equipped with Cu K $\alpha$  radiation ( $\lambda=1.5410 \text{ \AA}$ ) operating at 40 kV and 30 mA. Data were collected in a scanning mode in steps between 4° and 75° (2 $\theta$ ) with a step size of 0.05°/s. The basal distance was obtained using Bragg's Law.

Fourier-transform infrared spectroscopy (FTIR) spectra were collected on a Perkin Elmer Frontier FTIR spectrometer using KBr pellets containing 1% by weight of the samples. Analyses of all samples were performed in the range of 4000 to 400  $\text{cm}^{-1}$  with a resolution of 4  $\text{cm}^{-1}$ , accumulating 10 scans.

Absorbance measurements of the supernatant solutions were analyzed using a UV-Vis spectrophotometer (UV-1800 SHIMADZU) with a 1 cm path length glass cuvette at  $\lambda$  max nm (maximum absorbance).

Samples collected after the adsorption process had the electronic spectra analyzed using an Ocean Optics USB-2000 instrument for solid samples with a tungsten lamp in the range of 200–800 nm in diffuse reflectance mode.

Powder and paint-applied samples were analyzed by colorimetry, based on the CieLab system, using a portable colorimeter (NR60CP – 3NH).

The oxidation state and elemental composition of the samples were evaluated using X-ray photoelectron spectroscopy (XPS) with a PHI Genesis instrument from Physical Electronics (Chanhassen, MN, USA), equipped with a monochromatic Al K $\alpha$  X-ray source. The binding energy was calibrated based on the C 1s peak at 284.6 eV.



Laser-induced breakdown spectroscopy (LIBS) analyses were carried out by Applied Spectra J200 equipment. The clay samples were pelletized in circular discs of 1.2 cm and approximately 0.2-0.3 cm of height. The discs were prepared using 5 mg of each sample, and then it was pressed at 10 tons. The spectra were collected under air atmosphere between 186 and 1050 nm using a laser line at 50 % as source performing 10 shots per spot with 50  $\mu\text{m}$  of diameter and gate delay of 0.5  $\mu\text{s}$ .

The powder particle size distribution measurements were assessed by a Static Laser Scattering (SLS) Horiba LA-960 equipment using a 15 mL cuvette accessory and water as dispersion medium. The refractive index was set to 1.640 for red and blue lines.

### 3.0 Results and Discussions

Figure 1 shows the particle distribution for the SM, SMPH, and SMOx samples. The average particle size for the sample SM was 11.71  $\mu\text{m}$ . The SMPH and SMOx samples presented different particle size distributions, so the average particle size D50 for them was 0.18  $\mu\text{m}$  and 62.20  $\mu\text{m}$ , respectively. These values indicate that the clay aggregates are dissociated and well dispersed, as shown in the study by Yang et al. (2023) [9].

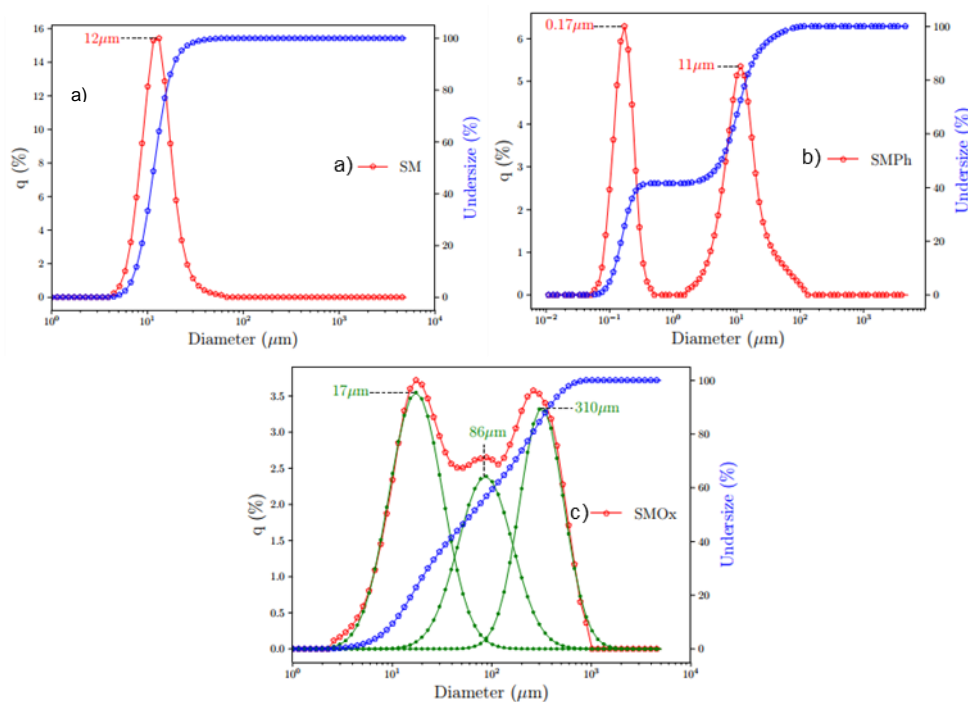
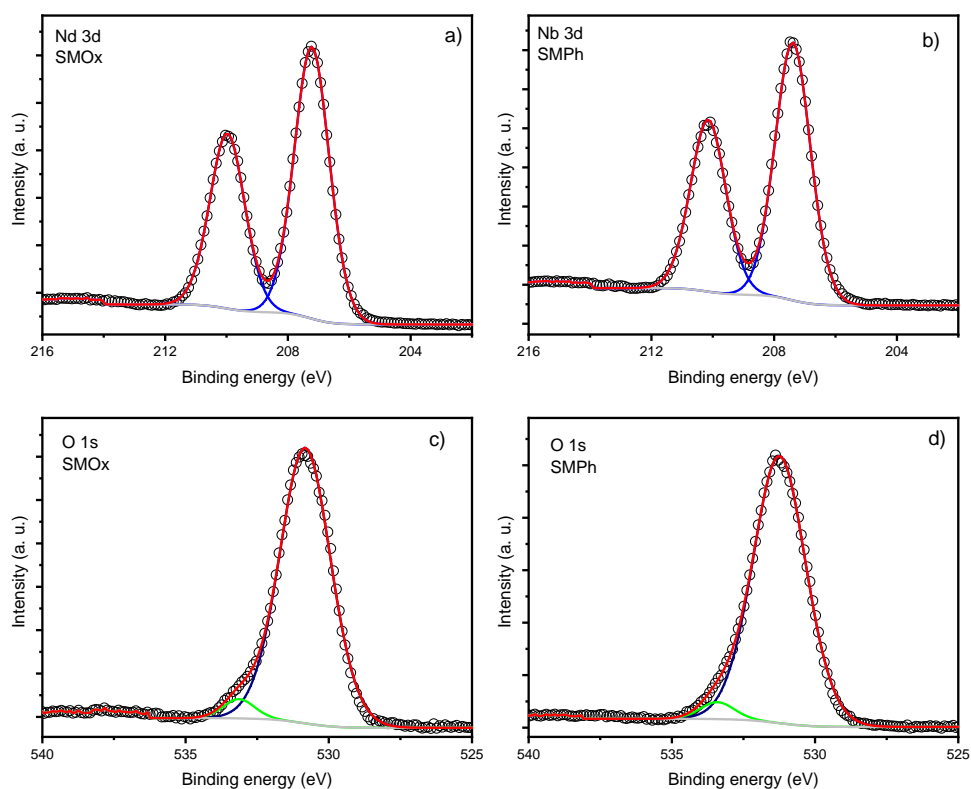


Figure 1. Particle size distribution for the samples SM (a), SMPH (b) and SMOx (c).

Figure 2 shows the X-ray photoelectron spectroscopy (XPS) analysis of niobium in SMOx and SMPH samples (Figures 2 a and b, respectively). The Nb 3d spectra exhibit two distinct peaks centered at 207.5 eV and 210.2 eV, corresponding to Nb 3d<sub>5/2</sub> and Nb 3d<sub>3/2</sub>, respectively, indicative of niobium +5. The O 1s XPS spectra are shown in Figure 2c for SMOx and Figure 2d for SMPH. The spectra of samples SMOx and SMPH are reproduced with two components centered at 530.9 and 533.5 eV. The component centered at 531.0 eV can be attributed to photoelectrons emitted from oxygen atoms in Si–O, Al–O, or Nb–O bonds, whereas the low-intensity component at higher binding energy can be associated with the hydroxyl OH<sup>-</sup> group of Nb–OH located in the interlayer region of the clay. Figure 2e shows the O1s spectrum recorded on sample SM. The high-intensity component centered at 532.0 eV is associated with oxygen bonds in Si-O-Si bonds [10].



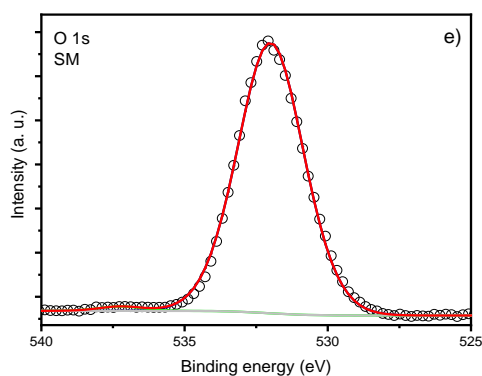


Figure 2: Photoelectron spectroscopy (XPS) spectra for Nb3d (a and b for the samples SMOx and SMPH, respectively), O 1s (c, d and e for the samples SMOx, SMPH and SM respectively).

Table 1 presents the chemical compositional analysis of the samples SM, SMOx, and SMPH determined by XPS. The results indicate that the smectite clay modified with niobium phosphate (SMPH) exhibit a phosphorous content of 2.0 % (wt %), thereby confirming the successful modification of the clay with this niobium compound. Furthermore, the samples, SMOx and SMPH, displayed niobium relative concentrations of 6.4 wt% and 4.0 wt%, respectively. These results suggest the incorporation of niobium into the clay matrix.

Table 1: Composition of the samples SM, SMOx, and SMPH determined by XPS.

Samples	wt (%)											
	C	N	O	F	Na	Mg	Al	Si	P	Ca	Nb	Fe
<b>SMOx</b>	6.4	-	62.5	1.1	2.6	2.1	4.8	13.1	-	1.0	6.4	-
<b>SMPH</b>	7.9	1.5	62.7	1.0	1.7	1.3	4.4	12.5	2.0	1.0	4.0	-
<b>SM</b>	9.3	-	55.0	-	6.0	3.8	6.5	17.5	-	1.4		0.5

In recent years, laser-induced breakdown spectroscopy (LIBS), an optical emission spectroscopic technique, has emerged as a rapid qualitative and quantitative analysis [11]. This spectroscopic technique can be explained by the short-duration, high-intensity pulsed laser being focused on a material, producing a plasma called laser-induced plasma (LIP) [11]. Qualitative and quantitative information about a sample is obtained by measuring the spectral delivery of the laser-induced plasma [11].

Figure 3 shows LIBS spectra for the samples SM, SMPH and SMOx. It is observed that the samples containing niobium show a higher density of spectral lines.

For the sample SM, the principal emissions lines for Mg, Al, Na, at around 279 nm, 309 nm and 589 nm, respectively, are consistent for the montmorillonite structure, and these results are coherent with XPS composition in Table 1. The modification of the clay samples with niobium was characterized by the presence of many other lines throughout the spectrum region, which highlighted the lines at 666 nm. XPS analysis (Table 1) as well as the XRD results (Figure 4) verified that the niobium compounds ( $\text{NbOPO}_4$  and  $\text{Nb}_2\text{O}_5$ ) were intercalated in the interlayer space of the clay. LIBS results showed the presence of lines of Mg and Na, at around 280 nm and 819 nm, respectively. As demonstrated in Table 1, the compositions of Mg and Na were reduced when the SM sample was modified with niobium compounds.

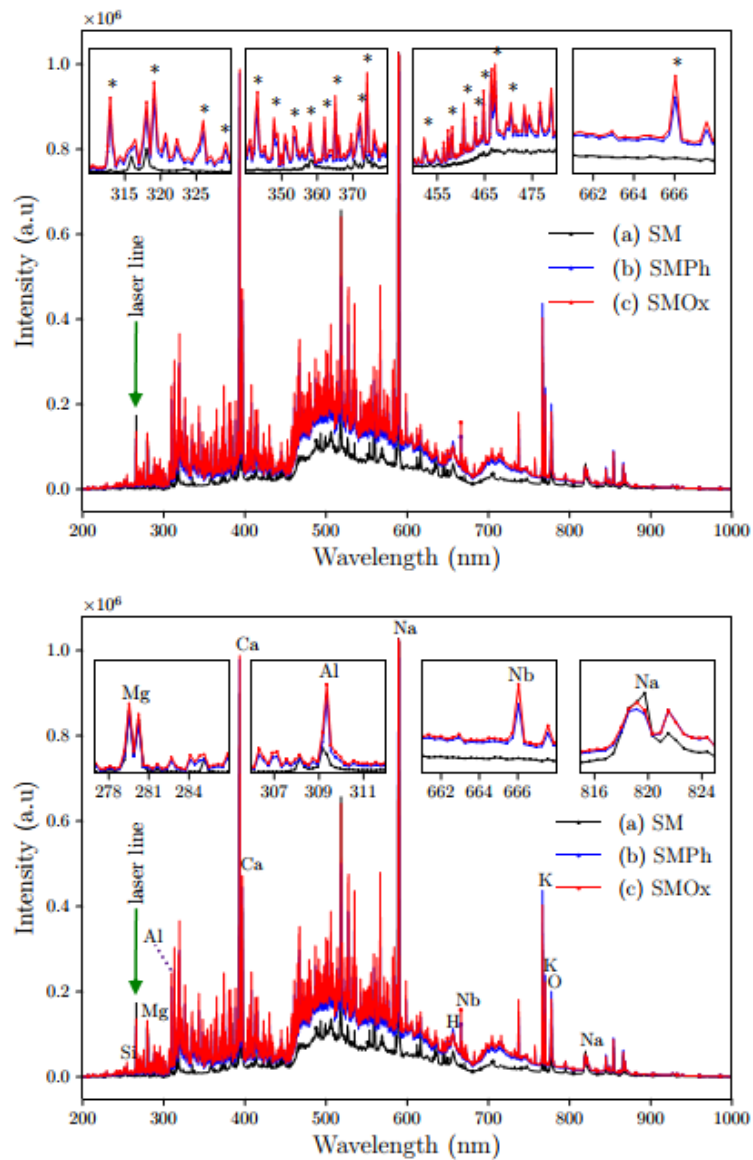


Figure 3: Laser-induced breakdown spectroscopy (LIBS) analysis for the samples SM (a), SMPH(b) and SMOx (c).

The X-ray diffraction (XRD) profile for smectite clay and its modifications with niobium phosphate and niobium oxide (SMPH and SMOx, respectively), as well as the samples obtained after adsorption/photocatalysis of MB (A-SMPH, A-SMOx, A-SMPHP, A-SMOxP), are shown in Figure 4. The XRD analysis for smectite before modification with niobium indicates dioctahedral montmorillonite (M-COD 9002779  $\text{Al}_2\text{Na}_{0.5}\text{O}_{12}\text{Si}_4$ ) with an amount of kaolinite (K-COD 1011045  $\text{Al}_2\text{H}_4\text{O}_9\text{Si}_2$ ) and quartz (Q-COD 9012600  $\text{SiO}_2$ ) at 13.8%, 41.6%, and 44.6%, respectively.

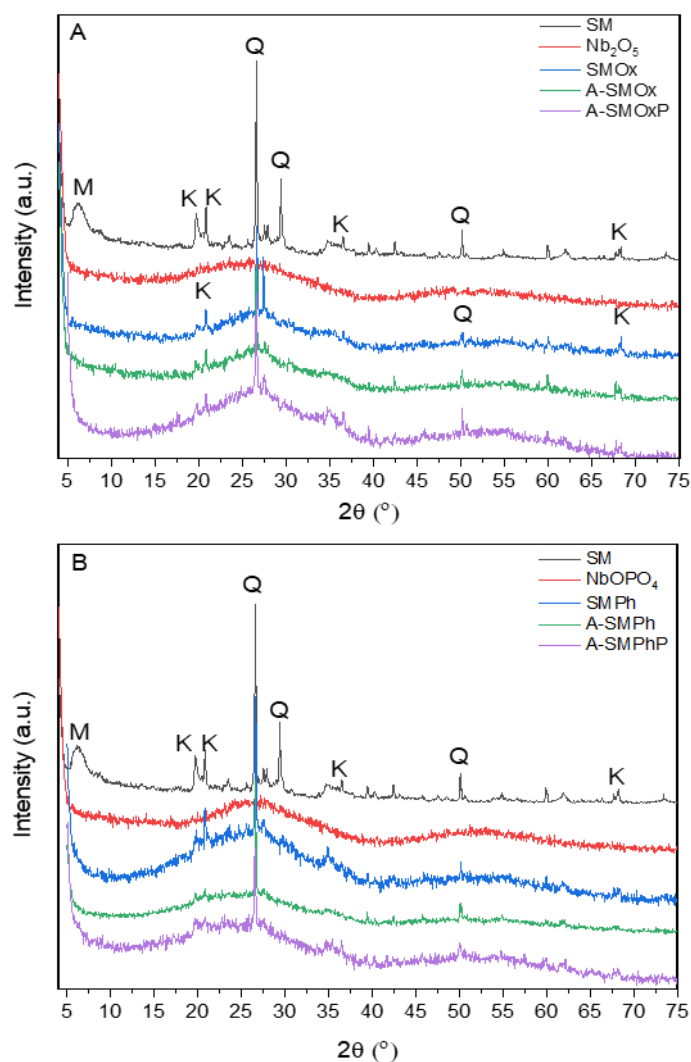


Figure 4: X-ray diffraction patterns of the smectite samples and those modified with Niobium Oxide (A) and Niobium Phosphate (B)

A similar diffraction profile for iron-rich bentonite was observed by Fontaine et al., 2020 [13]. The characteristic reflections of montmorillonite for the basal spacing correspond to approximately 15 Å ( $d_{001} = 14.88$  Å), related to the interlayer distance of 2:1 clays, resulting in a spacing between 14.0 Å - 15.0 Å [14]. The quartz phase was identified by the presence of reflections at  $2\theta = 20.96^\circ$ ,  $26.64^\circ$ , and  $50.02^\circ$ . The characteristic peaks that allowed the identification of the kaolinite phase were at  $2\theta = 12.48^\circ$ ,  $20.14^\circ$ ,  $25.63^\circ$ , and  $36.48^\circ$ .

Figure 4.a,b presents diffraction patterns with amorphous characteristics of the niobium compounds NbOPO<sub>4</sub> and Nb<sub>2</sub>O<sub>5</sub>. Two broad peaks were identified, one at approximately  $25.54^\circ$  ( $2\theta$ ) and the other at  $49.73^\circ$  ( $2\theta$ ) [14,15]. The amorphous pattern characteristic of niobium compounds was maintained upon modification of the smectite

clay with these compounds. For these compounds, was observed that the characteristic reflection of the (001) basal stacking plane of montmorillonite appeared to shift towards lower  $2\theta$  values (below 5 ( $2\theta$ ) values), indicating intercalation of  $\text{Nb}_2\text{O}_5$  and  $\text{NbOPO}_4$  structures, for the samples SMOx and SMPH, respectively.

Furthermore, characteristic peaks corresponding to the quartz and kaolinite phases were observed at reflections at  $2\theta = 20.14^\circ$  and  $68.5^\circ$  (phase K),  $26.64^\circ$  and  $50.02^\circ$  (phase Q). It can be observed that for the A-SMPH, A-SMOx, A-SMPHP, and A-SMOxP samples, those obtained after adsorption/photocatalysis of MB, the basal stacking (001) reflection shifted towards higher  $2\theta$  values compared to the clay modified with niobium but without MB. Beyond the displacement of the basal stacking (001) reflection of the sample SM, the results suggest that the  $\text{Nb}_2\text{O}_5$  and  $\text{NbOPO}_4$  structures, also the MB were intercalated between the clay layers, due to the reduced Na and Si elements, as observed in LIBS (Figure 1) results and XPS composition (Table 1 and Figure 2).

The Fourier-transform infrared spectroscopy (FTIR) spectra of the smectites before and after modification with niobium are shown in Figure 5. It can be observed that for the SM samples and all those modified with  $\text{NbOPO}_4$  (Figure 5 A), the spectra show a narrow band in the region of  $3638\text{ cm}^{-1}$ , associated with the (Al-OH-Al)  $\text{Al}_2\text{OH}$  vibrational stretching, indicative of smectite with a high aluminum content in octahedra [7,16]. The spectra for the  $\text{NbOPO}_4$  samples and the smectites modified with niobium phosphate (SMPH) before and after adsorption/photocatalysis (Figure 5A) show a band in the region of  $1043\text{ cm}^{-1}$ , due to the vibrational mode ( $\nu$ ) of asymmetric stretching of the phosphate ion.

The broadband in the region of  $3385\text{ cm}^{-1}$  and the narrow band in the region of  $1600$  or  $1637\text{ cm}^{-1}$  present in the spectrum for SM and the clay samples modified with  $\text{NbOPO}_4$  and  $\text{Nb}_2\text{O}_5$  are attributed to the stretching of hydroxyl (OH) and angular deformation of water molecule ( $\text{H}_2\text{O}$ ), respectively [7,17]. The band in the region of approximately  $1115\text{ cm}^{-1}$  is related to the stretching vibrations of Si-O. Bands in the region of  $520$  and  $463\text{ cm}^{-1}$ , which appear in all spectra of smectites and smectites modified with niobium, are attributed to the stretching and bending of Si-O present in the clay layers [7].

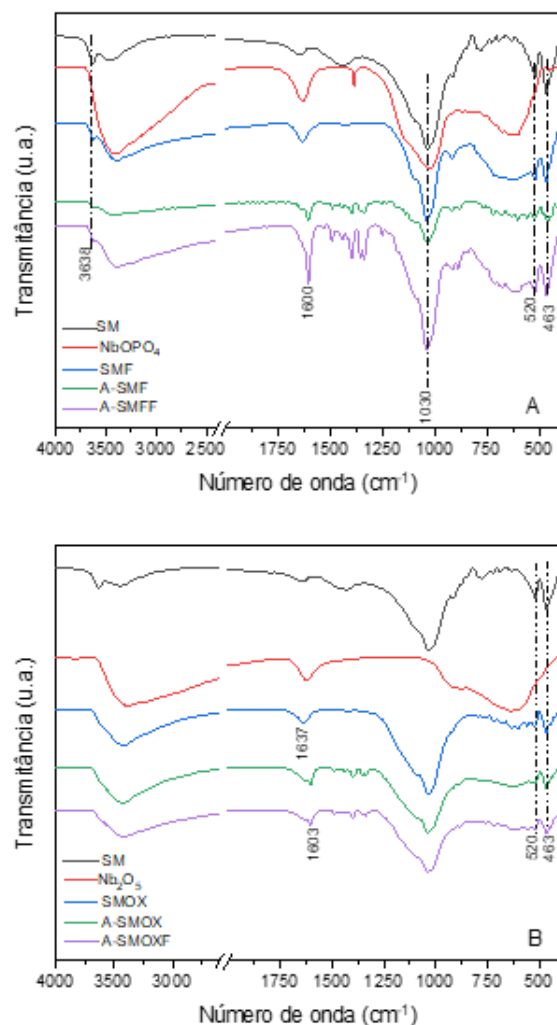


Figure 5: FTIR spectra for the smectite samples modified with Niobium phosphate (A) and Niobium oxide (B).

The spectra for Nb<sub>2</sub>O<sub>5</sub> and NbOPO<sub>4</sub> and the smectites modified with niobium before and after adsorption/photocatalysis present an intense band in the region of 630 cm<sup>-1</sup> related to the stretching of the Nb-O bond. The A-SMPh, A-SMPhP, A-SMOx, and A-SMOxP samples exhibit a set of bands in the region from 1477 to 1277 cm<sup>-1</sup> typical for the identification of the MB dye, indicating the intercalation of the dye between the layer of clay [18].

The absorbance spectra profiles in the visible region for the smectite samples and smectites modified with niobium are presented in Figure 6. It can be observed that the NbOPO<sub>4</sub> and Nb<sub>2</sub>O<sub>5</sub> powder samples do not show an absorption band. However, the smectite modified with these compounds exhibited a band with a maximum of 493 nm. The samples SMOx e SMPh obtained after adsorption/photocatalysis present



profiles like SM clay, with intense absorption in the UV region with a sharp drop of around 550 nm [8]. This fact indicates the feasibility of activating the A-SMPh, A-SMPhP, A-SMOx, and A-SMOXPh samples under visible light (above 400 nm) [8].

The indirect band-gap energy values for the SM, SMPh, SMOx, A-SMPhP, and A-SMOxP samples were estimated by the Tauc method [19]. The band gap values are presented in Table 2. The band-gap value of the SM sample (2.23 eV) was slightly higher than for the NbOPO<sub>4</sub> and Nb<sub>2</sub>O<sub>5</sub> compounds. The SMPh and SMOx samples modified with niobium remained with band-gap values close to those of the clay, 2.22 and 2.23 eV, respectively.

However, the values of the smectite samples modified with niobium recorded (A-SMPhP and A-SMOxP) after the photocatalysis experiment showed much lower values, namely 1.53 eV for the A-SMPhP and A-SMOxP samples (Table 2). The decrease in values occurred due to the smectite clay with small band-gap values, which generated impurity energy levels above the valence band edge. This results in lower energy values required to excite charge carriers, reducing the optical band [20].

Table 2: Band-gap values.

<b>Sample</b>	<b>Band-gap values</b>	<b>Sample</b>	<b>Band-gap values</b>
SM	2.23	---	---
NbO(PO <sub>4</sub> )	2.12	Nb <sub>2</sub> O <sub>5</sub>	2.21
SMPh	2.23	SMOx	2.22
A-SMPhP	1.53	A-SMOxP	1.53

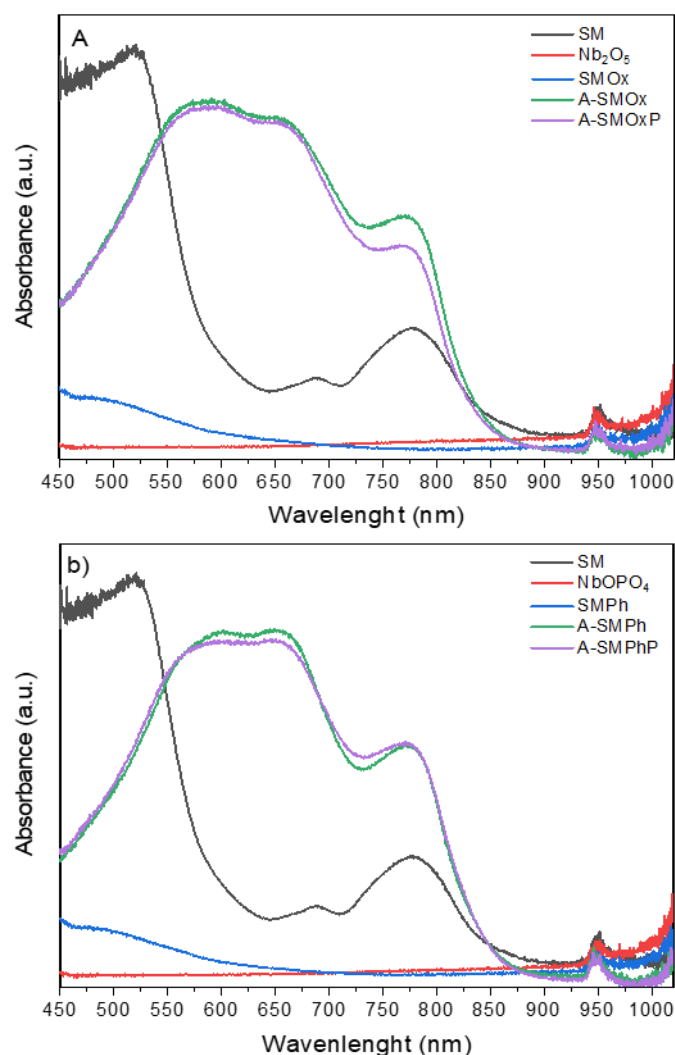


Figure 6: The absorbance spectrum in the visible region for the samples of smectite and their modifications with Niobium Oxide (A) and Niobium Phosphate(B).

Figures 7 show the comparison of the results obtained regarding the percentage of removal from adsorption and heterogeneous photocatalysis tests. The photocatalysis mechanism can be explained as follows: a semiconductor such as the SMPH and SMOx samples absorbs a photon, promoting an electron from the valence band ( $V_B$ ) to the conduction band ( $C_B$ ), creating a hole in the valence band ( $h_{BV}^+$ ) [8]. These holes induce the oxidative decomposition of organic molecules adsorbed on the catalytic surface. They also react with water molecules, producing the hydroxyl radical ( $OH\cdot$ ). This radical rapidly attacks the dye molecules in the solution, leading to mineralization into  $CO_2$  and  $H_2O$  [8].

According to the observed results, the SMOx and SMPH samples exhibited notably higher efficiency in the adsorption process (99.01% and 99.99%, respectively) compared to photocatalysis. This phenomenon can be attributed to the negative

surface charge of the modified clays SMOx and SMPH, which exhibit a strong affinity with the positively charged structure of the MB dye. On the other hand, the SMOx and SMPH samples demonstrated significant efficacy in MB removal, with removal rates of 94.5% and 99.81%, respectively. The preferential electron-hole ( $h_{BV}^+$ ) favoring of the SMOx catalyst hindered its photocatalytic activity [8].

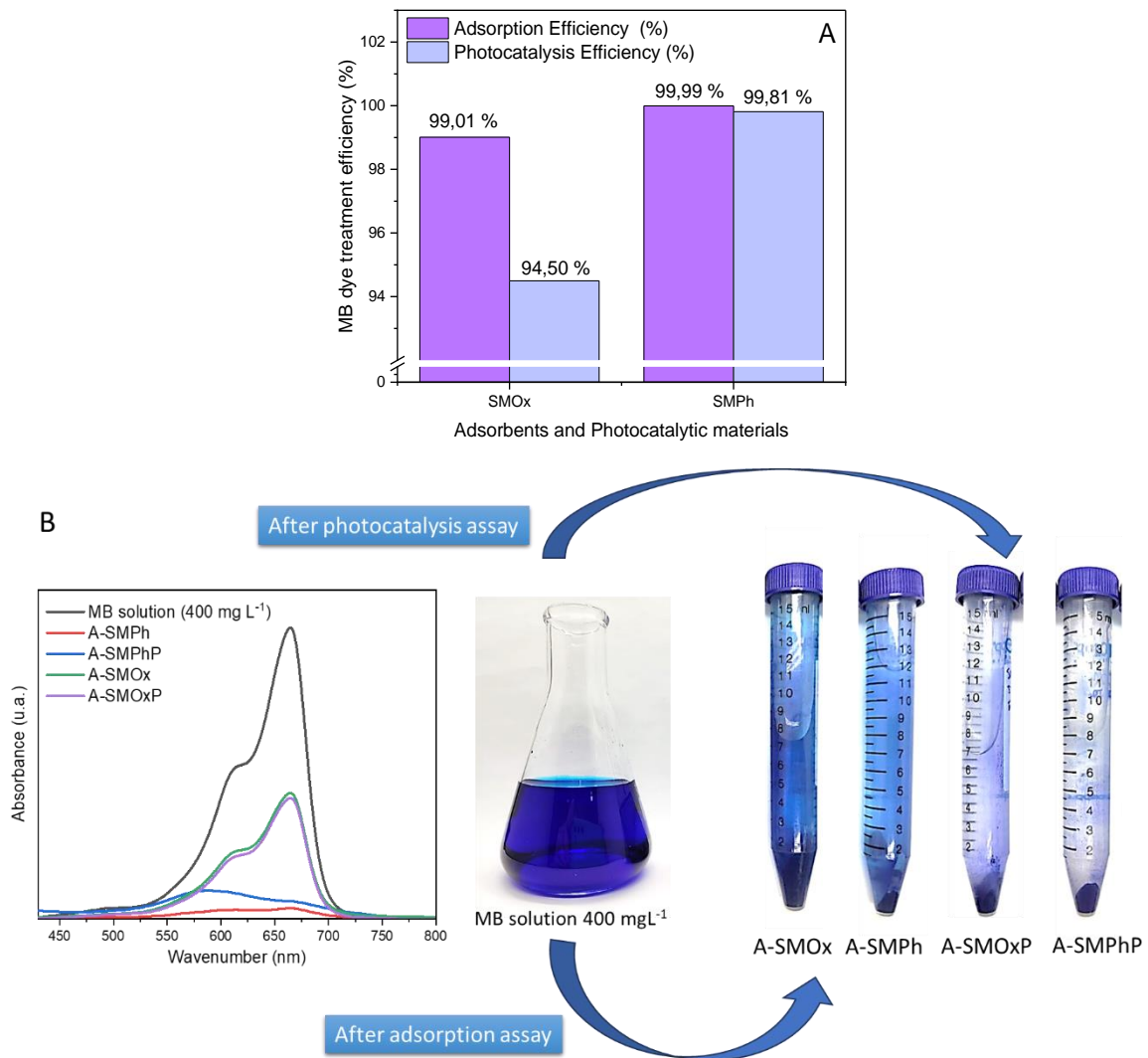


Figure 7: Adsorption and photocatalysis efficiency (A) and UV-Vis spectra following the digital images of the MB solutions after adsorption and photocatalysis assays (B) using the starting materials SMOx and SMPH.

In a study by Asencios et al. (2019) [8], niobium-modified clay was explored for the photocatalysis of Rhodamine B dye, yielding removal rates close to 95% removal. Additionally, Lacerda et al. (2020) [21] achieved up to 90% efficiency in the removal of reactive blue 19 dye using niobium-modified bentonite. These reports

demonstrate that the material obtained in this study presents high values of MB removal under UV light, standing out as a novel material.

The absorbance profiles of the niobium-modified samples dispersed in clear paint are shown in Figure S1. It is possible to observe that the SMOx and SMPH samples dispersed in clear paint, despite presenting a yellow coloration, did not show absorption bands. The samples collected after the adsorption/photocatalysis assays exhibited bands in the maximum region at 664 nm, corresponding to the  $\pi \rightarrow \pi^*$  electronic transitions of the adsorbed MB dye [22].

Tables 3 -4 and Figures S2-S3 present the values of the CIE L\*a\*b\* colorimetric parameters for the samples SMOx and SMPH (powder sample, cycle) even as they disperse in colorless paint (paint sample, square), respectively. The tables also include color difference values between the samples in powder form and those dispersed in colorless paint. Colorless paint does not contain white pigment in its matrix, enhancing the dispersed pigments' color. The  $\Delta E$  parameter quantified the color difference between two samples, SMOx and SMPH in powder form and those dispersed in colorless paint. As observed, the results of  $\Delta E$  shows that the samples A-SMPHP (12.17) and SMOx (9.82) before the adsorption/ photocatalysis process when dispersed in colorless paint demonstrate strong color parameter difference ( $\Delta E = 6 - 12$ ). The  $\Delta E$  values obtained for the samples SMPH (13.62) before the adsorption/ photocatalysis process, A-SMPH (23.38), A-SMOx (15.97) and A-SMOxP (13.80) were above 12, indicating a very strong color parameter difference [23].

The colorimetric parameters presented in Tables 3-4 and in Figures S2-S3 demonstrate that the test specimens painted with niobium-modified clay before the adsorption/photocatalysis of MB show higher luminosity (L). When the clay samples were colored MB, after the adsorption/photocatalysis process, the luminosity decreased. The A-SMPHP sample show a slight tendency towards green coloration (-a\*). On the other hand, when evaluating the b\* parameter, it is observed that all samples obtained after adsorption/photocatalysis of MB (A-SMPH, A-SMPHP, A-SMOx and A-SMOxP), whether in powder form or dispersed in paint, show a tendency towards blue coloration, as observed in the negative b\* values.

Table 3: Colorimetric parameters obtained by the CieLab system for the SMPh samples before and after the adsorption/photocatalysis assays in powder form (circle) and dispersed in paint colorless (square).




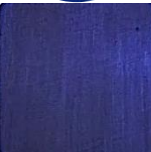




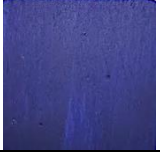

Sample	Colorimetric Parameters					$\Delta E$	Images of the sample
	L*	a*	b*	C*	h		
SMP <sub>h</sub>	77.02	2.47	10.38	10.67	76.67	-	
SMP <sub>h</sub>	90.54	2.19	12.03	12.23	68.01	13.62	
A-SMP <sub>h</sub>	13.45	4.91	-36.34	36.67	277.69	-	
A-SMP <sub>h</sub>	32.05	3.15	-22.29	22.51	278.05	23.38	
A-SMP <sub>h</sub> P	31.91	-5.08	-21.03	21.63	256.42	-	
A-SMP <sub>h</sub> P	32.98	5.97	-26.01	26.68	282.92	12.17	

Table 4: Colorimetric parameters obtained by the CieLab system for the SMPh samples before and after the adsorption/photocatalysis assays in powder form (circle) and dispersed in paint colorless (square).

Sample	Colorimetric Parameters					$\Delta E$	Images of the sample
	L	a*	b*	C*	h		
SMO <sub>x</sub>	80.96	3.07	13.17	11.05	73.85	-	
SMO <sub>x</sub>	90.42	0.71	12.03	9.63	85.78	9.82	

A-SMOx	22.91	13.94	-36.80	39.55	290.74	-	
A-SMOx	30.93	6.79	-24.99	25.90	285.20	15.97	
A-SMOxP	18.25	7.90	-30.06	31.00	284.72	-	
A-SMOxP	30.65	7.15	-24.06	25.10	286.54	13.80	

The SMPH, SMOx, A-SMPH, A-SMOx, A-SMPH<sub>P</sub>, A-SMOx<sub>P</sub> samples were evaluated for their in vitro antibacterial capacity using the minimum inhibitory concentration (MIC) method against the pathogenic bacteria *Proteus mirabilis* and *Bacillus cereus*. The results obtained are presented in Table 5

Table 5: MIC (mg/mL) for the in vitro antibacterial activity in water.

Sample	SMPH	SMOx	A-SMPH	A-SMOx	A-SMPH <sub>P</sub>	A-SMOx <sub>P</sub>
MIC <i>P. mirabilis</i>	*	*	0.31	0.31	0.15	0.62

\* MIC values were not determined

The samples A-SMPH, A-SMPH<sub>P</sub>, A-SMOx, and A-SMOx<sub>P</sub> demonstrated antibacterial activity against the *Proteus mirabilis* bacterial strains, with minimum inhibitory concentration (MIC) values recorded at 0.31, 0.15, 0.31, and 0.62 mg/mL, respectively. In contrast, the SMPH and SMOx samples exhibited no inhibitory effects at the tested concentrations for this microorganism.

The A-SMPH<sub>P</sub> sample exhibited the best MIC value at 0.15 mg/mL. In comparison, the A-SMPH sample, which did not undergo the photocatalysis process, demonstrated an MIC of 0.31 mg/mL. This indicates that the antibacterial activity for A-SMPH was approximately twice as high, suggesting that the photocatalytic process may enhance inhibitory efficiency. In contrast, the A-SMOx<sub>P</sub> sample yielded an MIC of 0.62 mg/mL, while its precursor, the A-SMOx which lacked photocatalytic treatment,

had an MIC of 0.31 mg/mL, indicating a more effective antibacterial action against the tested strains.

It is noteworthy that antibacterial activity was only observed in materials that had the addition of methylene blue, highlighting the influence of the dye on the assay outcomes. According to Thesnaar (2021) [24], many studies have demonstrated that methylene blue, either alone or in combination with other compounds, possesses antibacterial activity; however, the precise mechanism of action remains unclear. The SMPH, SMOx, A-SMPH, A-SMOx, A-SMPH<sub>P</sub>, and A-SMOx<sub>P</sub> samples did not exhibit minimum inhibitory activity against the other studied bacterial strain, *Bacillus cereus*.

These results highlight the selectivity of the studied samples (A-SMPH, A-SMPH<sub>P</sub>, A-SMOx, and A-SMOx<sub>P</sub>) in inhibiting Gram-negative bacteria, which typically exhibit increased resistance due to the presence of an outer membrane that protects them from certain antimicrobial agents [25]. Therefore, the preliminary results indicate that smectite clay modification with niobium oxide (SMOx) and niobium phosphate (SMPH), when adsorbed and/or photocatalyzed for the treatment of wastewater containing MB, demonstrates promising selective antibacterial activity against Gram-negative bacteria.

## 4.0 Conclusions

In conclusion, the presented study demonstrates that the modification of smectite clay with niobium phosphate and niobium oxide can be achieved through a simple and low-cost procedure. The XRD results revealed that the raw smectite contains additional phases such as kaolinite and quartz. The modified smectite clay with niobium (SMPH and SMOx) retained the amorphous characteristic typical of niobium compounds, as indicated by the XRD results. Furthermore, analyses using XPS and LIBS confirmed that the niobium compounds were intercalated in the clay structure.

The smectite sample, along with the SMPH and SMOx samples, exhibited adsorption and photocatalytic efficiencies exceeding 99 % for the removal of MB in water. This process resulted in a final product blue colored as evidenced by the colorimetric parameters obtained through the Ciel\*a\*b\* color space. The samples derived from the adsorption/photocatalysis tests (A-SMPH, A-SMPH<sub>P</sub>, A-SMOx, and

A-SMOxP) demonstrate significant antibacterial activity against the Gram-negative bacteria *Proteus mirabilis*, highlighting the influence of the dye in the assay outcomes.

The implications of this work extend to the development of a novel hybrid pigment. This pigment, synthesized from abundant natural clays of the Guarapuava region in conjunction with niobium, an abundant metal in Brazil, is easily synthesized, cost-effective and has potential as a pigment in commercial paints. Moreover, it exhibits antibacterial properties against pathogens responsible for various diseases, including ocular and auditory infections.

## Acknowledgments

The authors would like to thank the following agencies for their support: Capes, CNPq, Finep, and Fundação Araucária. S.J . is thankful for a CNPq PDJ post-doctorate grant (152230/2022-0). The authors also thank Dr. Andressa dos Santos for the colorimetric analysis. The structural drawings contained in the Graphical Abstract were produced using the VESTA software (Version 3), <https://jp-minerals.org/vesta/en/download.html> [28].

## References

1. Samandari, S.S., Samandari, S.S., Joneidi-Yekta, H., Mohseni, M. *Chemical Engineering Journal*, **308** , 1133–1144.
2. Bingül, Z. *Journal of Molecular Structure*, **2022**, 1250, 31729.
3. Nayl, A., Abd-Elhamid, A., Arafa, W.A.A., Ahmed, I.M., AbdEl-Rahman, A.M.E., Soliman, H.M.A., Ali, A.H.M. A., Aly, A.A., Bräse, S. *Materials*, **2023**, 16, 514.
4. Ma, L., Islam, S.M., Xiao, C., Zhao, J., Liu, H., Yuan, M., Sun, G., Li, H., Ma, S. Kanatzidis, M.G. *Journal of American Chemistry Society*, **2017**, 139, 12745–12757.
5. Li, K., Zheng, Z., Feng, J., Zhang, J., Luo, X., Zhao, G., Huang, X. *Journal of Hazardous Materials*, **1999**, 166,1180–1185
6. Akhtar, J.; Amin, N. A. S.; Shahzad, K. *Desalination and Water Treatment*, **2017**, 57, 12842–12860.



7. Rocha, M.L., Balaba, N., Jaeger, S.,Primo, J.O., Horsth, D.F.L., Appelt, P. Meneguzzi, D., Cunha, M. A.A., Anaissi, F.J. *Minerals*, **2023**, 13, 785.
8. Asencios, Y.J.O., Quijo, M.V., Marco, F.C.F., Nogueira, A.E., Rocca, R.R., Assaf, E.M. *Solar Energy*, **2019**, 194, 37–46.
9. Yang, T., Wang, N., Gu, H. *Applied Clay Science*, **2023**, 235 ,106866.
10. Qiu, G., Huang, C., Sun, X., Chen, B. *Green Chemistry*, **2019**, 21, 3930–3939.
11. Singh. P., Mal, E., Khare, A., Sharma, S. *Journal of Cultural Heritage*, **2018**, 33 ,71–82.
12. Fontaine, F., Christidis, G.E., Yans, J., Hollanders, S., Hoffman, A., Fagel, N. *Applied Clay Science*, **2020**, 187 ,105444.
13. Chen, J., Lu, J., Su, L., Ruan, H., Zhao, Y., Lee, C., Cai, Z., Wu, Z., Jiang, Y. *Applied Science*, **2022**, 12, 3182.
14. Marin, L.M., Hallet-Tapley, G.L., Impellizzeri, S., Fasciani, C., Simoncelli, S., Ferreira, J.C.N., Scaiano, J.C. *Catalysis Science and Technology*, **2014**,4, 3044.
15. Liang, F., Wu, D., Jiang, L., Zhang, Z., Zhang, W., Rui, Y., Tang, B., Liu, F. *ACS Applied Materials and Interfaces*, **2021**, 13, 51057–51065.
16. Madejová, J. FTIR techniques in clay mineral studies. *Vibrational Spectroscopy*, **2003**, 31,1–10.
17. Zhang, Y., Wang, J.,Ren, J., Liu, X., Li, X., Xia, Y., Lu, G., Wang, Y. *Catalysis Science Technology*, **2012**, 2, 2485–2491.
18. Raiyaan, G.D., Kalith, S.B.M., Sheriff, M.A., Arunachalam, K.D. *Journal of Aquaculture and Marine Biology*, **2021**,10,146-150.
19. Borht, K.W., Galdino, C.W., Teixeira, V. C., Anaissi, F.J. *Applied Surface Science*, **2021**, 546,149126.
20. Zainab, S., Azeem, M., Awan, S.U., Rizwan, S., Iqbal, N., Rashid, J. *Scientific Reports*, **2023**, 13, 6954.
21. Lacerda, E.H.C., Monteiro, F.C., Kloss, J.R., Fujiwara, S. T. *Journal of Photochemistry & Photobiology A: Chemistry*, **2020**, 388,112084.
22. Kostjukova, L. O.; Leontieva, S. V.; Kostjukov, V. V. *Journal of Molecular Liquids*, **2021**, 336, 116369.

23. Quindici, M. **O Segredo das Cores**. São Paulo: All Print Editora, 2013.
24. Thesnaar, L., Bezuidenhout, J.K., Petzer, A., Petzer, J.P., Cloete, T. *Journal of Pharmaceutical Sciences*, **2021**, 157, 105603.
25. Ramachandran, G. *Virulence*, **2014**, 5, 213-218.
26. Clinical and Laboratory Standards Institute (CLSI). *Methods for Dilution Methods for Dilution Antimicrobial Susceptibility Tests for Bacteria that Grow Aerobically*. 11th ed. **CLSI standard M07** (ISBN 1-56238-836-3 [Print]; ISBN 1-56238-837-1 [Electronic]). Clinical and Laboratory Standards Institute, 950 West Valley Road, Suite 2500, Wayne, Pennsylvania 19087, USA, 2018.
27. Balouiri, M.; Sadiki, M.; Ibsouda, S.K. *Journal of Pharmaceutial Analysis*, **2016**, 6,71–79.
28. Momma, K., Izumi, F. *Journal of Applied Crystallography*, 2011, 4, 1272-1276.